

# HAWK-INSPIRED COOPERATIVE ENCIRCLEMENT GUIDANCE OF FIXED-WING UAV SWARM WITH LIMITED COMMUNICATION IN THREAT SCENARIO

Boyu QIN1, Dong ZHANG2 & Shuo TANG3

School of Astronautics, Northwestern Polytechnical University, Xi'an, China Shaanxi Aerospace Flight Vehicle Design Key Laboratory, Xi'an, China

#### **Abstract**

This paper tackles the challenging problem of safety-critical cooperative guidance of the fixed-wing unmanned aerial vehicle (UAV) swarm system with limited interaction for dynamic target encirclement. In the task scenario, several non-cooperative flight vehicles threaten the UAV flight safety and intend to prevent the encirclement. A hawk-inspired multi-layer framework is proposed in this work to guide the UAV swarm to safely encircle the target. Each layer copes with a decomposed guidance subproblem. Firstly, an online cooperative allocation for each UAV's blockading area is implemented with the modeled Harris hawk swarm's hunting criteria adopted. Secondly, the Hawks' predation strategy is employed as the cooperative pursuit guidance law based on the UAV nonlinear dynamics model and multi-threat interception model. Besides, a control barrier function (CBF) for non-cooperative scenario based on the three-dimensional (3D) Velocity Obstacle (VO) is designed to achieve safety penetration. The proposed approach is scalable and adaptive due to adopting distributed decision-making and control modes to support large-scale UAV swarm engagement amidst limited communication. Finally, numerical simulations are carried out to demonstrate the effectiveness of the proposed multi-layer cooperative guidance framework of the limited-communicating UAV swarm for the target encirclement under multiple threats.

**Keywords:** Distributed fixed-wing UAV swarm, cooperative encirclement guidance, safety-critical control, limited communication

## 1. Introduction

Recently, unmanned aerial vehicle (UAV) has drawn intensive attention due to its benefit of commanding a large-scale group of UAVs to simultaneously accomplish missions in various military or industrial fields, e.g., geographical mapping, search and rescue, and disaster inspection [1, 2]. For the deployed multiple UAVs in various scenarios, cooperative flight is a fundamental and vital ability to efficiently perform different tasks [3, 4]. Cooperative encirclement guidance is one of vital and practical issues for the application of UAV swarm. The encirclement posture can effectively support the fixed-wing UAV swarm to implement omni-directional and strong real-time sensing towards targets in three-dimensional space, or to carry out multi-angle interception [5, 6].

Up to now, to the best of our knowledge, the cooperative guidance for the fixed-wing UAV swarm to encircle the dynamic target in threat scenarios under constrained interaction has not been efficiently addressed. Different from some unmanned systems with the general theoretical model like the unicycle system analyzed in most of the previous literature, fixed-wing UAVs have complex and special dynamics characteristics and are sensible to the model used in methods. Thus, some existing works cannot meet the requirement of the model matching and are unable to be directly applied [7]. Meanwhile, for some typical existing approaches, such as cooperative differential games [8] and multi-agent reinforcement learning [9], the cost of calculation resources and time on data mining, policy learning, and online solving will explosively grow up with the increase of the swarm scale and

the dimension of the vehicle states. All the above restrictions indicate the inappropriateness of applying existing work for the UAV swarm cooperative encirclement guidance. To promote the research level of the swarm application, it has essential to develop a convenient, fast, and low-cost scheme for the cooperative encirclement guidance of fixed-wing UAV swarm.

To establish the vital bridge between the cooperative encirclement guidance and the UAV swarm with limited communication, it is essential to address the following 4 key issues: (1) The encirclement guidance strategy needs to consider the coupling constraints of the UAV dynamics to match the UAV motion characteristics. (2) An efficient guidance needs to be established to guide the UAV to achieve the coverage of dynamic target areas through autonomous coordination based on the capabilities and resources of the UAV swarm. (3) The time synchronization of each UAV's behavior should be ensured to avoid the encirclement omissions. (4) Flight conflicts in the limited-interacting UAV swarm crucially ought to be dissipated to guarantee the flight safety of each individual UAV, and simultaneously the collisions with external non-cooperative threats must be avoided by the swarm.

To remedy the above problems, this paper draws inspiration from the Harris' Hawks' coordinated hunting behavior [10], establishing a novel multi-layer guidance framework for UAV swarm. Each layer is respectively designed for one of the decomposed subproblems including the blockading area allocation, spatially-temporally cooperative guidance and flight safety coordination. In the upper layer, the online cooperative allocation for each UAV's blockading area is implemented with the modeled Harris' hawk swarm's hunting criteria so that the corresponding task efficiency function is quantitatively designed. In the middle layer, a pursuit guidance law is correspondingly proposed by imitating the Hawk's maneuver behavior of chasing prey. Besides, a distributed coordination mechanism is introduced to adjust each UAV's time-to-go under the limited communication network and achieve the spatial-time synchronization for the swarm. Subsequently, in the lower layer, distributed safety-critical maneuver control strategy is proposed to deal with collaborative UAVs and non-collaborative threats. A novel control barrier function (CBF) based on Velocity Obstacle (VO) is applied to obtain the threat avoidance and the flight safety of the UAV swarm. As the further step, the safe maneuver control of each UAV can be then calculated by solving a constrained QP problem of the optimal revision for the designed nominal control input.

This work benefits the research on flexible and safety-critical cooperative guidance of the fixed-wing UAV swarm. According to the literature investigation result, our work is the first attempt to study the bionic cooperative guidance framework for the fixed-wing UAV swarm to encircle the dynamic target in threat scenarios under constrained communication, which fills the blank of the research in the swarm encirclement problem and provides a new reference to the application of the bionic swarm intelligence theory to the unmanned system.

#### 2. Problem Formulation

## 2.1 Fixed-wing UAV Swarm Model

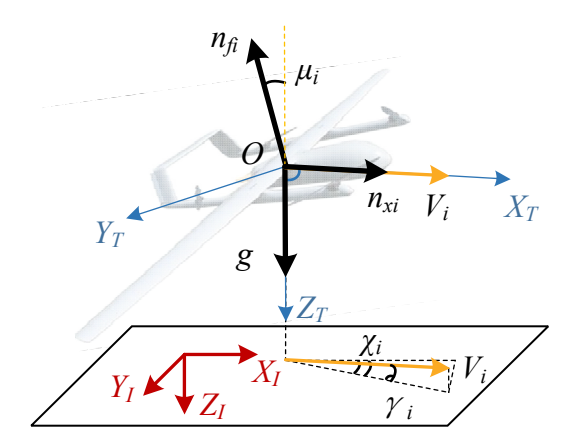


Figure 1 – The coordinate system and UAV flight dynamics variables

The dynamics variables of the fixed-wing UAV model adopted in this article is a 3-DOF model shown in Figure 1. In what follows, the model assumes that the autopilot can stabilize the UAV attitude. It is also assumed that the earth is flat and the fuel expenditure is negligible. Under these

assumptions, the 3-DOF dynamics model [11] can be described by

$$\begin{cases} \dot{x}_{i} = V_{i} \cos \gamma_{i} \cos \chi_{i} \\ \dot{y}_{i} = V_{i} \cos \gamma_{i} \sin \chi_{i} \\ \dot{z}_{i} = -V_{i} \sin \gamma_{i} \\ \dot{V}_{i} = g \left( n_{xi} - \sin \gamma_{i} \right) \\ \dot{\chi}_{i} = \frac{g}{V_{i} \cos \gamma_{i}} n_{fi} \sin \mu_{i} \\ \dot{\gamma}_{i} = \frac{g}{V_{i}} \left( n_{fi} \cos \mu_{i} - \cos \gamma_{i} \right) \end{cases}$$

$$(1)$$

where  $p_i = [x_i, y_i, z_i]^T$  and  $v_i = [x_i, y_i, z_i]^T$  denotes the position and velocity of UAV i in the earth-surface inertial coordinate  $OX_IY_IZ_I$ , respectively.  $[V_i, \chi_i, \gamma_i]^T$  are the speed, path angle and heading angle of UAV i, respectively.  $[n_{xi}, n_{fi}, \mu_i]^T$  are tangential load, normal load and bank angle, respectively, which are the control inputs of the UAV model.  $g = 9.8 \text{ m/s}^2$  is the gravity acceleration.

The above model is inconvenient to apply when designing the guidance law. Therefore, a guidance-oriented model is established by coordinate transformation, and one can obtain

$$\begin{cases} \dot{p}_i = v_i \\ \dot{v}_i = u_i \end{cases} \tag{2}$$

where  $\mathbf{u}_i = [u_{ix}, u_{iy}, u_{iz}]^T$  is the virtual control, while  $\mathbf{v}_i = [v_{ix}, v_{iy}, v_{iz}]^T$  is denoted as the velocity vector. According to (1)-(2), the mathematical relation between the virtual control vector  $\mathbf{u}_i$  and the real control input vector  $[n_{xi}, n_{fi}, \mu_i]^T$  is

$$\mathbf{u}_{i} = g \begin{bmatrix} \cos \gamma_{i} \cos \chi_{i} & -\sin \chi_{i} & \sin \gamma_{i} \cos \chi_{i} \\ \cos \gamma_{i} \sin \chi_{i} & \cos \chi_{i} & \sin \gamma_{i} \sin \chi_{i} \\ -\sin \gamma_{i} & 0 & \cos \gamma_{i} \end{bmatrix} \begin{bmatrix} n_{xi} \\ n_{fi} \sin \mu_{i} \\ -n_{fi} \cos \mu_{i} \end{bmatrix} + \begin{bmatrix} 0 \\ 0 \\ 1 \end{bmatrix}$$
(3)

Thus, one can render that

$$n_{xi} = \Gamma_{i1}, \ n_{fi} = \sqrt{\Gamma_{i2}^2 + \Gamma_{i3}^2}, \ \mu_i = \arctan\left(\frac{\Gamma_{i2}}{-\Gamma_{i3}}\right)$$
 (4)

where  $\boldsymbol{\varGamma}_i = [\Gamma_{i1}, \Gamma_{i2}, \Gamma_{i3}]^T$  and

$$\boldsymbol{\Gamma}_{i} = \frac{1}{g} \begin{bmatrix}
\cos \gamma_{i} \cos \chi_{i} & -\sin \chi_{i} & \sin \gamma_{i} \cos \chi_{i} \\
\cos \gamma_{i} \sin \chi_{i} & \cos \chi_{i} & \sin \gamma_{i} \sin \chi_{i} \\
-\sin \gamma_{i} & 0 & \cos \gamma_{i}
\end{bmatrix}^{T} \begin{pmatrix} \boldsymbol{u}_{i} - \begin{bmatrix} 0 \\ 0 \\ g \end{bmatrix} \end{pmatrix}$$
(5)

Once the virtual control  $u_i$  is calculated by the designed guidance law, the corresponding maneuver command of UAV i can be obtained by (4) and (5).

The limited communication topology can be described by the following undirected graph

$$C = \begin{bmatrix} c_{11} & c_{12} & \cdots & c_{1n} \\ c_{21} & c_{22} & \cdots & c_{2n} \\ \vdots & \vdots & \ddots & \vdots \\ c_{n1} & c_{n2} & \cdots & c_{nn} \end{bmatrix}, c_{ij} = \begin{cases} 0, & \| \boldsymbol{p}_i - \boldsymbol{p}_j \| > D_{com} \\ 1, & \| \boldsymbol{p}_i - \boldsymbol{p}_j \| \le D_{com} \end{cases} (i, j = 1, 2, \dots n)$$
(6)

where n is the number of UAVs, C is the adjacency matrix, of which each element  $c_{ij}$  represents the communication state between UAV i and j, and  $D_{com}$  is the communication range. This model is applied for all the subsequent subproblems relevant to the distributed decision, planning and control.

#### 2.2 Multi-threat Interception Model

To efficiently and conveniently describe the threat motion, one can adopt the following model

$$\begin{cases}
\dot{\boldsymbol{p}}_{th,j} = \boldsymbol{v}_{th,j} \\
\dot{\boldsymbol{v}}_{th,j} = \boldsymbol{u}_{th,j}
\end{cases}$$
(7)

where  $u_{oj}$  is the threat's acceleration control input. Moreover, three maneuver criteria are designed to simulate the interception, including the attack toward the UAV, and the collision avoidance with other threats. Therefore, the maneuver strategy of the threat during the interception can be designed as follows

$$\boldsymbol{u}_{th,j} = \boldsymbol{u}_{th,att,j} + \boldsymbol{u}_{th,avo,j} \tag{8}$$

where  $u_{th,att,j}$  represents the attack behavior, and  $u_{th,avo,j}$  is the collision avoidance input.

The attack component  $u_{th,att,j}$  is shown as follows, which simulates the threat tendency to approach the UAV swarm. The attack occurs when UAVs enter the threat's detection area. Once finding UAVs, threats are accelerated by the attraction of UAVs producing a motion similar to pure pursuit. The attack finishes when the relative distance is lower than an attack-available tolerance.

$$\boldsymbol{u}_{th,att,j} = \sum_{i \in \mathcal{A}_{j}} \left( k_{ap,ji} \frac{\boldsymbol{p}_{i} - \boldsymbol{p}_{th,j}}{\|\boldsymbol{p}_{i} - \boldsymbol{p}_{th,j}\|} + k_{av,ji} \frac{\boldsymbol{v}_{i} - \boldsymbol{v}_{th,j}}{\|\boldsymbol{v}_{i} - \boldsymbol{v}_{th,j}\|} \right)$$
(9)

where

$$k_{ap,ji} = K_{ap} e^{\frac{1+\frac{\|\boldsymbol{p}_i - \boldsymbol{p}_{th,j}\|^2}{D_{det,thr}^2}}, \ k_{av,ji} = K_{av} e^{\frac{1+\frac{\|\boldsymbol{p}_i - \boldsymbol{p}_{th,j}\|^2}{D_{det,thr}^2}}, \ \mathcal{A}_j = \left\{i \| \boldsymbol{p}_i - \boldsymbol{p}_{th,j} \| \le D_{det,thr} \right\}$$

$$(10)$$

where  $D_{det,thr}$  is the detection radius,  $k_{ap,ji}$ ,  $k_{av,ji}$  are the attack gains, in which  $K_{ap}$ ,  $K_{av}$  are constants.

The collision avoidance component drives the threats to keep away from each other with a certain distance. This component works if there are other threats within the safety radius of a threat. The maneuver command is expressed as follows

$$\mathbf{u}_{th,avo,j} = \sum_{k \in \mathcal{A}_j} k_{sp,jk} \frac{\mathbf{p}_{th,j} - \mathbf{p}_{th,k}}{\|\mathbf{p}_{th,j} - \mathbf{p}_{th,k}\|}$$
(11)

where  $k_{s,jk}$  is the avoidance gain expressed by

$$k_{sp,jk} = K_{sp} \frac{D_{safe,th} - \left\| \boldsymbol{p}_{th,j} - \boldsymbol{p}_{th,k} \right\|}{D_{safe,th}}$$
(12)

where  $K_s$  is constant,  $R_{Aj}$  is the safety radius, and  $k_{s,ij}$  is an adaptive avoidance gain with respect to the relative distance. The formulation of the multi-threat interception model complete here.

#### 2.3 Control Barrier Function (CBF)

Before moving forward, Control barrier function (CBF) is introduced with their application in the context of safety. Consider a nonlinear system in the affine form

$$\dot{\mathbf{x}} = f(\mathbf{x}) + g(\mathbf{x})\mathbf{u} \tag{13}$$

where  $x \in \mathcal{D} \subseteq \mathbb{R}^n$  is the state, and  $u \in U \subseteq \mathbb{R}^n$  is the input for the system. Assume that the functions  $f: \mathbb{R}^n \to \mathbb{R}^n$  and  $g: \mathbb{R}^n \to \mathbb{R}^{n \times m}$  are continuously differentiable. Define a forward invariance set  $\mathcal{S} \subseteq \mathcal{D}$  of a continuously differentiable function  $h: \mathcal{D} \subseteq \mathbb{R}^n \to \mathbb{R}$  yielding

$$S = \left\{ x \in \mathcal{D} \subseteq \mathbb{R}^n \middle| h(x) \ge 0 \right\} \tag{14}$$

$$\partial S = \left\{ x \in \mathcal{D} \subseteq \mathbb{R}^n \middle| h(x) = 0 \right\}$$
 (15)

$$\operatorname{Int}(\mathcal{S}) = \left\{ \mathbf{x} \in \mathcal{D} \subseteq \mathbb{R}^n \middle| h(\mathbf{x}) > 0 \right\}$$
 (16)

Definition 1 [12] (Control Barrier Function): Given the set  $\mathcal{S}$  defined by ()-(), with  $\frac{\partial h(x)}{\partial x^T} \neq \mathbf{0}$ ,  $\forall x \in \partial \mathcal{S}$ ,

the function h is called the control barrier function (CBF) defined on the set D, if there exists an

extended class  $\mathcal{K}$ , the function  $\kappa$  such that for all  $x \in \mathcal{D}$ 

$$\sup_{\boldsymbol{u}\in\mathbb{U}}\left[\underbrace{L_f h(\boldsymbol{x}) + L_g h(\boldsymbol{x})\boldsymbol{u}}_{h(\boldsymbol{x})} + \kappa(h(\boldsymbol{x}))\right] \ge 0 \tag{17}$$

where  $L_f h(x) = \frac{\partial h(x)}{\partial x^T} f(x)$  and  $L_g h(x) = \frac{\partial h(x)}{\partial x^T} g(x)$  are the Lie-derivatives.

For the further step, various constraints based on CBF that the system must satisfy can be established by both the geometry and dynamics analysis. To restrict the state within the constraints, a Quadratic Programming (QP) formulation can be established for the safety of the system. And CBFs are generally used as safety filters which modifies the nominal input for tasks in a minimal way:

$$\mathbf{u}^*(\mathbf{x},t) = \min_{\mathbf{u} \in \mathbb{U} \subseteq \mathbb{R}^m} \|\mathbf{u} - \mathbf{u}_{nom}\|^2$$
s.t.  $L_f h(\mathbf{x}) + L_e h(\mathbf{x}) u + \kappa(h(\mathbf{x})) \ge 0$  (18)

The above problem is called the Control Barrier Function based Quadratic Program (CBF-QP). The existing work [13] prove that the explicit solution of the CBF-QP problem is given by

$$u^{*}(x,t) = u_{nom}(x,t) + u_{safe}(x,t)$$
 (19)

where  $u_{safe}$  is obtained by

$$\mathbf{u}_{safe}(\mathbf{x},t) = -\frac{L_g h(\mathbf{x})^T}{L_g h(\mathbf{x}) L_g h(\mathbf{x})^T} \min(0, \ \psi(\mathbf{x},t))$$
(20)

where  $\psi(x,t) = \dot{h}(x,u_{nom}(x,t)) + \gamma(h(x))$ . The sign of  $\psi(x,t)$  indicates whether the safety constraint activates, yielding that the control law switch based on the safety situation.

## 3. Multi-layer Bionic Guidance Framework

In this section, a multi-layer bionic guidance framework is established as the UAV swarm tactics to cooperatively and safely encircle the dynamic target. First, the swarm blockade allocation is modelled based on hawks' swarm hunting criteria. Then, the hawks' predation strategy is correspondingly employed as the cooperative pursuit guidance law. After that, a control barrier function (CBF) based on the 3D Velocity Obstacle (VO) is designed to cope with the multi-threat interception and achieve the safety penetration. The whole framework is shown as Figure 2.

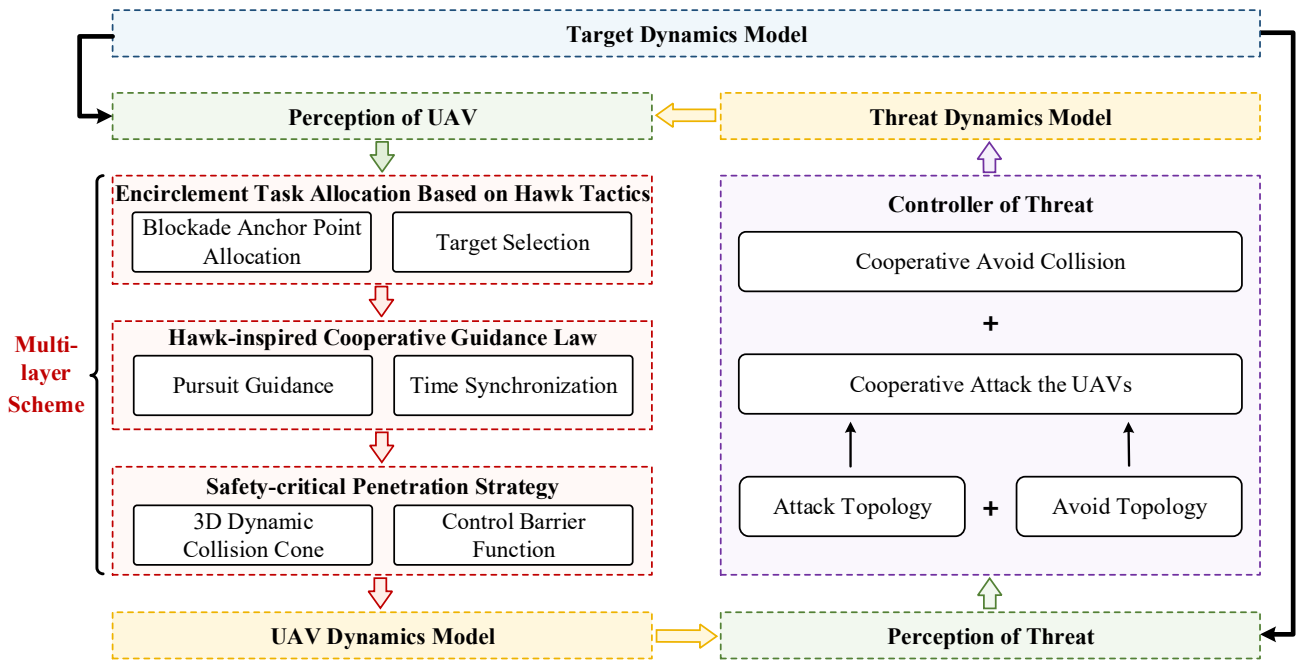


Figure 2 – The diagram of the multi-layer guidance framework

## 3.1 Encirclement Task Allocation Mechanism Based on Hawk Tactics

Researches of biological intelligence indicates that the hunting efficiency can be greatly improved when the hawk swarm adopt sophisticated tactics to encircle the prey groups. Before moving forward, the characteristics of the swarm hunting is firstly analyzed and illustrated.

Generally, the hunting process can be divided in two stages including blockade area allocation and target determination. For the former stage, each hawk shares the relevant task and flight information and equally negotiates with others within a limited range so that the blockade area of each hawk is assigned. For the latter, each hawk evaluates the value of preys in the allocated area and then decides the target prey with the largest value to pursue. Thus, the hawk-inspired encirclement tactics of UAV can be correspondingly designed with a two-stage strategy composed of the cooperative blockade area allocation and the target selection mechanism.

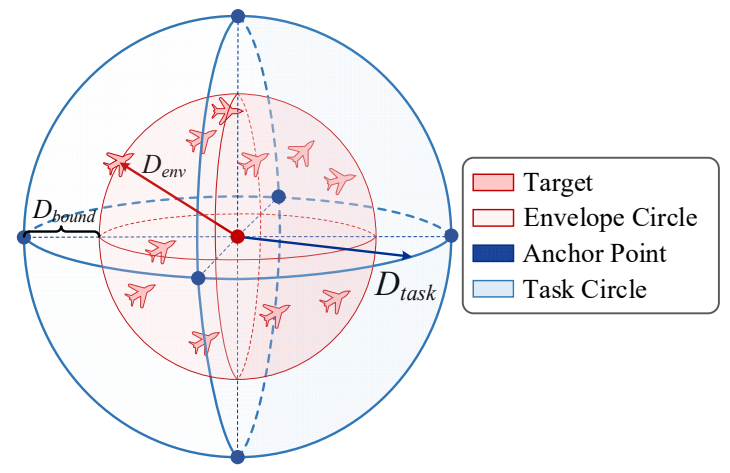


Figure 3 - The diagram of the modelled task area

#### 3.1.1 Blockade Anchor Point Allocation

The blockade allocation strategy begins with modelling the task area. To achieve the uniform and omni-directional encirclement, an envelope sphere surrounding all the preys is applied to describe the irregular spatial configuration of the prey swarm. In the sphere, the center  $p_{tg,c}$  is selected as the mean position of the swarm with  $N_{tg}$  targets and the radius  $D_{env}$  is the maximum of the distance between the center  $p_{tg,c}$  and the targets. Apart from the above, a boundary layer with a thickness  $D_{bound}$  is set at the outer of the sphere as a redundant space in case UAVs require when maneuvering to pursue the target. Thus, the modelled task area can be mathematically expressed as follows.

$$S: \left\| \boldsymbol{p} - \boldsymbol{p}_{tg,c} \right\| \le D_{task} \tag{21}$$

where

$$\boldsymbol{p}_{tg,c} = \frac{1}{N_{tg}} \sum_{j=1}^{N_{tg}} \boldsymbol{p}_{tg,j}, \ D_{task} = D_{env} + D_{bound}, \ D_{env} = \max_{j} (\|\boldsymbol{p}_{tg,j} - \boldsymbol{p}_{tg,c}\|)$$
 (22)

For the convenience of the subsequent allocation,  $N_{uav}$  anchor points  $\{\underline{\boldsymbol{p}_{env,m}}\}_{m=1}^{N_{univ}}$  uniformly distributed on the sphere are selected as the representation of the divided subarea so that the blockade area allocation problem is transferred to a problem of multiple points.

Moreover, the cooperation within a limited range indicates a distributed coordination of the swarm. Here, a distributed optimization approach based on Consensus-Based Bundle Algorithm (CBBA) is adopted to solve the optimization of the blockade area allocation. CBBA is a bidding-based method and divided into two phases: bundle building phase and consensus phase. In the bundle building phase, each UAV selects a task independently. The task bundle is constructed in accordance with the greedy principle. After that, the algorithm enters into the consensus phase, at which the UAV will receive the winning agent list, winning bid list, and timestamps information of other UAVs and share its own information. The concrete steps are detailed illustrated in [14].

To apply CBBA to blockade allocation, a score function  $B_{im}$  of each UAV for each anchor point  $p_{env.m}$ , which consists of the number of neighboring targets and distance discount, is here constructed as follows and treated as the optimization goal.

$$B_{im} = \frac{K_B \left| \mathcal{N}_{em} \right|}{\left\| \boldsymbol{p}_i - \boldsymbol{p}_{env,m} \right\|}, \ \mathcal{N}_{em} = \left\{ j \left\| \left\| \boldsymbol{p}_{tg,j} - \boldsymbol{p}_{env,m} \right\| \le D_{env} \right\} \right\}$$
(23)

where  $D_e$  is the considered maximum radius for each anchor point to determine the neighboring targets,  $K_B$  is a positive constant.

# 3.1.2 Target Selection

After the anchor point allocation, each UAV needs to further decide the target to pursue. Here a target selection mechanism is proposed. Through the observation and experiments, the target selection mechanism during the hawk's hunting can be concluded into three criteria: proximity criterion, margin criterion and density criterion [15]. Among these criteria, the proximity criterion indicates the hawk tends to choose the closest prey as its pursuit target. Denote the assigned target for UAV i as  $\tilde{p}_{env,i}$ . And the corresponding expression is as follows

$$T_{i1} = \underset{j \in \mathcal{N}_{env,i}}{\operatorname{arg\,min}} \left( \left\| \boldsymbol{p}_{tg,j} - \tilde{\boldsymbol{p}}_{env,i} \right\| \right), \ \mathcal{N}_{env,i} = \left\{ j \left\| \left\| \boldsymbol{p}_{tg,j} - \tilde{\boldsymbol{p}}_{env,i} \right\| \le D_{env} \right\} \right.$$

$$(24)$$

where  $T_{i1}$  is the selected target based on the proximity criterion.

The margin criterion implies the hawk prefer to select the most peripheral prey as the target. And relevant work [] shows that it is one of the most typical and vital hunting criteria to lessen the confusion effect when the prey merges into a flock.

$$T_{i2} = \underset{j \in \mathcal{N}_{env,i}}{\operatorname{arg\,max}} \left( \left\langle \frac{\boldsymbol{p}_{tg,j} - \boldsymbol{p}_{i}}{\left\| \boldsymbol{p}_{tg,j} - \boldsymbol{p}_{i} \right\|}, \frac{\boldsymbol{p}'_{ij}}{\left\| \boldsymbol{p}'_{tj} \right\|} \right\rangle \right), \, \, \mathcal{N}_{env,i} = \left\{ j \left\| \left\| \boldsymbol{p}_{tg,j} - \tilde{\boldsymbol{p}}_{env,i} \right\| \le D_{env} \right\} \right.$$

$$(25)$$

where  $T_{i2}$  is the selected target based on the margin criterion,  $D_{nei}$  is the considered radius for each target to determine the neighboring targets.

$$\boldsymbol{p}'_{tj} = \frac{1}{\left|\mathcal{N}_{nei,j}\right|} \sum_{k \in \mathcal{N}_{nei,j}} \frac{\boldsymbol{p}_{tg,j} - \boldsymbol{p}_{tg,k}}{\left\|\boldsymbol{p}_{tg,j} - \boldsymbol{p}_{tg,k}\right\|}, \, \, \mathcal{N}_{nei,j} = \left\{j \left\|\left\|\boldsymbol{p}_{tg,j} - \boldsymbol{p}_{tg,k}\right\| \le D_{nei}, k \ne j\right\}$$
(26)

The density criterion suggests that the hawk pursues the target located in the densest area. And in this work, we consider the hawk has priority to occupy the largest blank area. The density criterion can be mathematically expressed as

$$T_{i3} = \underset{j \in \mathcal{N}_{env,i}}{\operatorname{arg\,max}} \left( \frac{\boldsymbol{p}_{tg,j} - \overline{\boldsymbol{p}}_{tg,j}}{1 + e^{-|\mathcal{N}_{nei,j}|}} \right), \ \mathcal{N}_{env,i} = \left\{ j \left\| \left| \boldsymbol{p}_{tg,j} - \widetilde{\boldsymbol{p}}_{env,i} \right| \right| \le D_{env} \right\}, \mathcal{N}_{nei,j} = \left\{ j \left\| \left| \boldsymbol{p}_{tg,j} - \boldsymbol{p}_{tg,k} \right| \right| \le D_{nei}, k \neq j \right\}$$
(27)

where  $T_{i3}$  is the selected target based on the density criterion

$$\overline{\boldsymbol{p}}_{tg,j} = \frac{1}{\left|\mathcal{N}_{nei,j}\right|} \sum_{k \in \mathcal{N}_{nei,j}} \frac{\boldsymbol{p}_{tg,k}}{\left\|\boldsymbol{p}_{tg,k}\right\|}, \quad \mathcal{N}_{nei,j} = \left\{j \left\|\left\|\boldsymbol{p}_{tg,j} - \boldsymbol{p}_{tg,k}\right\| \le D_{nei}, k \ne j\right\}$$
(28)

Based on the above criteria, one can obtain three alternative targets. Then, a situation evaluation function is designed to decide the final target to pursue during the encirclement. Inspired by [16], the adopted evaluation function is composed of distance and orientation.

The distance is one of the most significant index terms directly reflecting the flight cost. The distance contribution  $J_{d,ij}$  can be defined as follows

$$J_{d,ij} = \frac{\|\boldsymbol{p}_i - \boldsymbol{p}_{tg,j}\|}{\frac{1}{3} \sum_{j \in T_i} \|\boldsymbol{p}_i - \boldsymbol{p}_{tg,j}\|}, \ T_i = \{T_{i1}, T_{i2}, T_{i3}\}$$
(29)

Besides, the guidance law tends to drive the UAV's velocity vector and the target's velocity vector to keep on the same orientation with LOS. Therefore, the larger the derivation angle between the two velocity vectors, the more the energy will cost during the pursuit maneuver. The orientation contribution  $J_{o,ij}$  is shown as follows.

$$J_{o,ij} = 1 - \frac{\left\langle \boldsymbol{\delta}_{i}, \, \boldsymbol{\delta}_{ij} \right\rangle}{\pi} \tag{30}$$

Incorporate both distance and orientation factors, the final evaluation shown in () can be obtained by the product of the above contributions

$$J_{ij} = J_{d,ij}J_{o,ij} \tag{31}$$

# 3.2 Hawk-inspired Cooperative Guidance Law

#### 3.2.1 Pursuit Guidance

After the determination of the target prey, each hawk will maneuver to hunt its target. Existing researches and tests [17] show that the hawk's pursuit behavior in three-dimensional (3D) space during the predation approximately obey a mixed guidance law combining the proportional navigation (PN) and proportional pursuit (PP). Inspired by the hawk's hunting dynamics, the cooperative pursuit law of UAV swarm can be designed to generate the real-time maneuver commands.

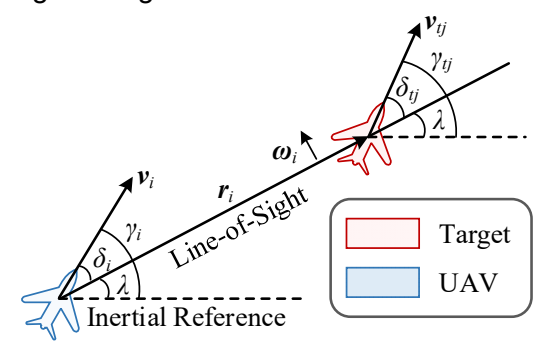


Figure 4 - Geometry of a pursuit

The hunting dynamics in 3D space can be modelled by the relative kinematics analysis between UAV i and the target  $T_i$  as shown in Figure 4, where  $p_i$  and  $p_{tg,i}$  are the position vectors, respectively. And  $v_i$  and  $v_{ti}$  are corresponding velocity vectors. Further,  $r_i$  is the Line-of-Sight (LOS) vector from UAV i to target  $T_i$ , of which the expression is

$$\mathbf{r}_i = \mathbf{p}_{tg,i} - \mathbf{p}_i \tag{32}$$

And the closing velocity vector  $v_{ci}$  is defined as

$$\mathbf{v}_{ci} = \mathbf{v}_i - \mathbf{v}_{tg,j} \tag{33}$$

Denote  $\delta_i$  as the deviation angle between  $v_i$  and  $r_i$ , then it can be given in vector form as

$$\boldsymbol{\delta}_{i} = \arccos\left(\frac{\boldsymbol{r}_{i} \cdot \boldsymbol{v}_{i}}{\|\boldsymbol{r}_{i}\| \cdot \|\boldsymbol{v}_{i}\|}\right) \cdot \left(\frac{\boldsymbol{r}_{i} \times \boldsymbol{v}_{i}}{\|\boldsymbol{r}_{i} \times \boldsymbol{v}_{i}\|}\right)$$
(34)

while the LOS rate is given in the following vector form as

$$\boldsymbol{\omega}_{i} = \frac{\boldsymbol{r}_{i} \times (-\boldsymbol{v}_{ci})}{\|\boldsymbol{r}_{i}\|^{2}} \tag{35}$$

Under the PN guidance, UAV *i* is commanded to maneuver at a rate proportional to the LOS rate, such that the PN component of the commanded acceleration can be obtained by

$$\boldsymbol{u}_{i,PN} = K_{i,PN} \left( \boldsymbol{\omega}_i \times \boldsymbol{v}_i \right) \tag{36}$$

where  $K_{i,PN}$  is the guidance gain of PN. Under the PP guidance, UAV i will turn at a rate proportional to the deviation angle. Thus, the PP component can be calculated by

$$\mathbf{u}_{i,PP} = K_{i,PP} \left( -\boldsymbol{\delta}_i \times \mathbf{v}_i \right) \tag{37}$$

where  $K_{i,PP}$  is the guidance gain of PP. Then, the total acceleration command of UAV i for the pursuit can be got by combining the two above elements

$$\boldsymbol{u}_{ip} = \boldsymbol{u}_{i,PN} + \boldsymbol{u}_{i,PP} = K_{i,PN} \left( \boldsymbol{\omega}_i \times \boldsymbol{v}_i \right) - K_{i,PP} \left( \boldsymbol{\delta}_i \times \boldsymbol{v}_i \right)$$
(38)

During the hunting, UAVs can real-time change their pursuit strategies by adaptively adjust the guidance gains. PN is almost the optimal guidance with less maneuver cost when the derivation angle  $\delta$  approximates to 0, whilst PP can rapidly eliminate  $\delta$  to 0 to guarantee the UAV's heading direction to point toward the target prey. Thus, an adaptive law of the guidance gain is designed as

$$\begin{cases}
K_{i,PN} = k_{pn}e^{-\|\delta_i\|} \\
K_{i,PP} = k_{pp}\left(1 - e^{-\|\delta_i\|}\right)
\end{cases}$$
(39)

where  $k_{pn}$  and  $k_{pp}$  are positive constants.

## 3.2.2 Time Synchronization Guidance

The above guidance law drives UAVs to fly towards the selected target so that the spatial cooperation can be realized. However, it cannot guarantee that UAVs will reach the assigned area at the same time to create a cooperative encirclement situation.

To address this issue, a time coordination mechanism is needed to achieve time synchronization of the swarm. It is an efficient approach to cooperatively control the time-to-go. Generally, the time-to-go of each UAV can be estimated by the following equation

$$\begin{cases} t_{go,i}(t) = -\frac{r_i(t)}{\dot{r}_i(t)} \\ r_i(t) = \left\| \boldsymbol{p}_i - \boldsymbol{p}_{tg,i} \right\| \\ \dot{r}_i(t) = \frac{\left(\boldsymbol{v}_i - \boldsymbol{v}_{tg,i}\right)^T \left(\boldsymbol{p}_i - \boldsymbol{p}_{tg,i}\right)}{\left\| \boldsymbol{p}_i - \boldsymbol{p}_{tg,i} \right\|} \end{cases}$$

$$(40)$$

where  $r_i$  is the norm of the LOS vector  $\mathbf{r}_i$  and  $\dot{r}_i$  is its rate. On this basis, a distributed time coordination mechanism is proposed. First, each UAV calculates its current time-to-go based on (9), and then broadcasts its time-to-go to the neighbor UAVs and receives the neighbors' time-to-go within a limited communication range. After that, select the average time-to-go of the local network as the desired time-to-go, and one can render that

$$\hat{t}_{go,i} = \frac{1}{|\mathcal{N}_i|} \sum_{j=1}^n c_{ij} t_{go,i}, \mathcal{N}_i = \left\{ j \middle| c_{ij} > 0 \right\}$$
(41)

Furthermore, each UAVs' desired speed can be correspondingly calculated as

$$\hat{V}_{i} = \frac{r_{i}}{\hat{t}_{go,i}} \cos \langle p_{i} - p_{tg,i}, v_{i} - v_{tg,i} \rangle = \frac{\left(p_{i} - p_{tg,i}\right)^{T} \left(v_{i} - v_{tg,i}\right)}{\hat{t}_{go,i} \left\|v_{i} - v_{tg,i}\right\|}$$
(42)

and then the axial load  $n_{xt,id}$  required to accelerate can be rendered as

$$n_{xt,id} = \frac{1}{g} \frac{\Delta V_i}{\Delta t} = \frac{1}{g} \frac{\hat{V}_i - V_i}{\Delta t}$$
 (43)

The discrete difference method shown in (13) may encounter derivative kicks in the application. Here a one-order low-pass filter is adopted to get the differential as well as the axial load  $n_{xt,ic}$ 

$$\begin{cases} \dot{S}_{it} = -\tau S_{it} + (\hat{V}_i - V_i) \\ n_{xt,ic} = \dot{S}_{it} / g \end{cases}$$
(44)

where  $S_{it}$  is the filter state and  $\tau$  is the time constant. For the further step, the input  $u_{it}$  for the time synchronization for in the Cartesian coordinate frame can be calculated as

$$\mathbf{u}_{it} = g(\mathbf{R}_{T \to I} [n_{xt,ic} \quad 0 \quad 0]^T + [0 \quad 0 \quad -1]^T)$$
(45)

To sum up, one can obtain the total acceleration command of UAV i for cooperative guidance

$$\boldsymbol{u}_{i,nom} = \boldsymbol{u}_{ip} + \boldsymbol{u}_{it} \tag{46}$$

## 3.3 Safety-critical Penetration Strategy

The above task-oriented guidance laws drive the UAV swarm to cooperatively achieve the encirclement of the target, but are unable to make UAVs actively avoid the noncooperative threats so that a safety-critical penetration strategy is required.

# 3.3.1 Three-dimensional Adaptive Velocity Obstacle

According to the requirement of UAV penetration, a certain safe distance should be maintained between UAV and the threat to avoid collision. If UAV is regarded as a particle and the threat is correspondingly "expanded", the threat avoidance during can be simplified as a particle evading the expansion circle. The main idea of velocity obstacle (VO) is to generate a conical obstacle interval, named Collision Cone (CC), in the velocity space of the UAV and guarantee the relative velocity vector to keep out of the CC.

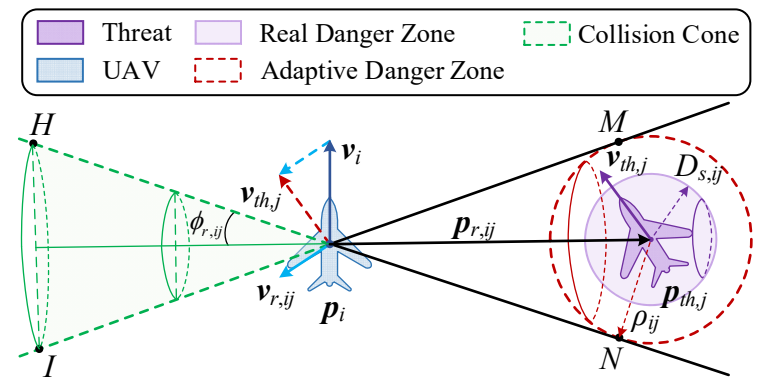


Figure 5 – Three-dimensional Collision Cone of UAV

The traditional speed obstacle method often only considers two-dimensional planes, and is inconvenient to apply in the three-dimensional flight scenario. Here, an adaptive 3D-VO for three-dimensional flight is designed and a geometric view is shown in Figure 5, where the green shaded area represents the 3D-VO set and indicates that the potential collision will happen in a short time if the velocity vector of the UAV is located in the shaded area.  $p_{th,j}$  and  $v_{th,j}$  are the position and velocity vector of the threat j;  $p_{r,ij} = p_{th,j} - p_i$  and  $v_{r,ij} = v_{th,j} - v_i$  are the relative position and velocity between UAV i and threat j, respectively;  $\phi_{r,ij}$  is denoted as the half vortex angle of the corresponding 3D Collision Cone, i.e., 3D-VO set;  $\rho_{ij}$  is defined as the radius of the adaptive danger zone. Here we select  $\rho_{ij} = \|p_{r,ij}\|^d / D_s^{d-1}$  to adaptively adjust the danger zone according to the real-time distance between the UAV and threat.

#### 3.3.2 CBF based Safety Controller

The approach begins with defining an appropriate CBF representative of typical dangers and events. A kind of distance-based CBF, i.e.,  $h_i(\mathbf{p}_i) = \|\mathbf{p}_i - \mathbf{p}_{th,j}\|^2 - \rho_{ij}^2$ , is widely applied in the collision avoidance of vehicles in some works [18, 19]. However, recent researches [20] prove that it is ineffective for fixed-wing UAVs with high-order dynamics due to only considering position relations.

To overcome the difficulty, here a novel CBF is constructed based on 3D Velocity Obstacle (3D-VO). The velocity information is introduced so that the impacts of the motion trend on UAV safety can be taken into account, and the CBF candidate is designed as

$$\begin{cases}
h_{i}(\boldsymbol{p}_{r,ij}, \boldsymbol{v}_{r,ij}) = \|\boldsymbol{p}_{r,ij}\| \|\boldsymbol{v}_{r,ij}\| \cos \phi_{r,ij} - \boldsymbol{p}_{r,ij}^{T}(-\boldsymbol{v}_{r,ij}) \\
\cos \phi_{r,ij} = \frac{\sqrt{\|\boldsymbol{p}_{r,ij}\|^{2} - \rho_{ij}^{2}}}{\|\boldsymbol{p}_{r,ii}\|}, \ \rho_{ij} = \frac{\|\boldsymbol{p}_{r,ij}\|^{d}}{D_{s}^{d-1}}
\end{cases} (47)$$

where  $\phi_{r,ij}$  is the half angle of the 3D-CC.

Before moving forward, since the UAV and threat do not collaborate and even form a game relation, only considering the UAV own control decision optimization cannot fully guarantee the safety. The influence of the threat behavior on UAV ought to be taken into account. Thus, here we reformulated the problem (18) as

$$u_{i}^{*}(x,t) = \min_{u \in \mathbb{U} \subseteq \mathbb{R}^{m}} \left\| u_{i} - u_{i,nom}(x) \right\|^{2}$$
s.t.  $L_{f}h(x) + L_{g}h^{i}(x)u_{i} + L_{g}h^{th,j}(x)u_{th,j} + \kappa(h(x)) \ge 0$ 

$$(48)$$

where  $L_g h^i(\mathbf{x})$  and  $L_g h^i(\mathbf{x})$  are the Lie-derivatives with respect to the UAV control input  $\mathbf{u}_i$  and the threat control input  $\mathbf{u}_{th,j}$ , respectively. Based on the above formulation, we have the following result. **Theorem 1**: Given the guidance-oriented UAV model (2)-(5), the proposed CBF candidate with defined by (16) is a valid CBF.

**Proof**: When there is  $\|\mathbf{v}_{r,ij}\| \neq 0$ , taking the derivative of (17) yields

$$\dot{h}_{i}(\boldsymbol{p}_{r,ij},\boldsymbol{v}_{r,ij}) = \frac{\sqrt{\|\boldsymbol{p}_{r,ij}\|^{2} - \rho_{ij}^{2}}}{\|\boldsymbol{v}_{r,ij}\|} \boldsymbol{v}_{r,ij}^{T} \dot{\boldsymbol{v}}_{r,ij} + \frac{\|\boldsymbol{v}_{r,ij}\|(\boldsymbol{p}_{r,ij}^{T} \dot{\boldsymbol{p}}_{r,ij} - \rho_{ij} \dot{\rho}_{ij})}{\sqrt{\|\boldsymbol{p}_{r,ij}\|^{2} - \rho_{ij}^{2}}} + \boldsymbol{v}_{r,ij}^{T} \dot{\boldsymbol{p}}_{r,ij} + \boldsymbol{p}_{r,ij}^{T} \dot{\boldsymbol{v}}_{r,ij} \tag{49}$$

According to (2), one can render

$$\begin{cases}
\dot{p}_{r,ij} = \dot{p}_{th,j} - \dot{p}_i = v_{th,j} - v_i = v_{r,ij} \\
\dot{v}_{r,ij} = \dot{v}_{th,j} - \dot{v}_i = u_{th,j} - u_i
\end{cases}$$
(50)

Substituting (49) into (48) yields that

$$\dot{h}(\boldsymbol{p}_{r,ij}, \boldsymbol{v}_{r,ij}) = \boldsymbol{v}_{r,ij}^{T} \boldsymbol{v}_{r,ij} + \frac{\|\boldsymbol{v}_{r,ij}\|(\boldsymbol{p}_{r,ij}^{T} \boldsymbol{v}_{r,ij} - \boldsymbol{\rho}_{ij} \dot{\boldsymbol{\rho}}_{ij})}{\sqrt{\|\boldsymbol{p}_{r,ij}\|^{2} - \boldsymbol{\rho}_{ij}^{2}}} + \underbrace{\left(-\frac{\sqrt{\|\boldsymbol{p}_{r,ij}\|^{2} - \boldsymbol{D}_{sj}^{2}}}{\|\boldsymbol{v}_{r,ij}\|} \boldsymbol{v}_{r,ij}^{T} \boldsymbol{u}_{i} - \boldsymbol{p}_{r,ij}^{T} \boldsymbol{u}_{i}\right)}_{L_{g}h^{I}(\boldsymbol{p}_{r,ij}, \boldsymbol{v}_{r,ij})} + \underbrace{\left(-\frac{\sqrt{\|\boldsymbol{p}_{r,ij}\|^{2} - \boldsymbol{D}_{sj}^{2}}}{\|\boldsymbol{v}_{r,ij}\|} \boldsymbol{v}_{r,ij}^{T} \boldsymbol{u}_{i}\right)}_{L_{g}h^{I}(\boldsymbol{p}_{r,ij}, \boldsymbol{v}_{r,ij})} \tag{51}$$

As the further step,  $\sup_{\pmb{u}_i \in \mathbb{U}} [\dot{h}_i(\pmb{p}_{r,ij},\pmb{v}_{r,ij}) + \kappa(h_i(\pmb{p}_{r,ij},\pmb{v}_{r,ij}))] \ge 0$  will be proved. Consider the worst case in which the derivation angle between  $\pmb{p}_{r,ij}$  and  $\pmb{v}_{r,ij}$  is  $(\pi - \phi_{r,ij})$ , and there is  $h_i(\pmb{p}_{r,ij},\pmb{v}_{r,ij}) = 0$  at this time. Next, define the derivation angle between  $\pmb{p}_{r,ij}$  and  $\pmb{u}_i$  as  $<\pmb{p}_{r,ij},\pmb{u}_i>\in(-\pi,\pi]$  and at the same time the derivation angle between  $\pmb{v}_{r,ij}$  and  $\pmb{u}_i$  is  $<\pmb{v}_{r,ij},\pmb{u}_i>\in(-\pi,\pi]$ . Then, one can render that

$$\sup_{\boldsymbol{u}_{i},\boldsymbol{u}_{j}\in\mathbb{U}} \left[ \dot{h}_{i}(\boldsymbol{p}_{r,ij},\boldsymbol{v}_{r,ij}) + \kappa(h_{i}(\boldsymbol{p}_{r,ij},\boldsymbol{v}_{r,ij})) \right] \\
= \sup_{\boldsymbol{u}_{i},\boldsymbol{u}_{j}\in\mathbb{U}} \left[ \boldsymbol{v}_{r,ij}^{T} \boldsymbol{v}_{r,ij} + \frac{\|\boldsymbol{v}_{r,ij}\|(\boldsymbol{p}_{r,ij}^{T} \boldsymbol{v}_{r,ij} - \rho_{ij}\dot{\rho}_{ij})}{\sqrt{\|\boldsymbol{p}_{r,ij}\|^{2} - \rho_{ij}^{2}}} + \left( -\frac{\sqrt{\|\boldsymbol{p}_{r,ij}\|^{2} - \rho_{ij}^{2}}}{\|\boldsymbol{v}_{r,ij}\|} \boldsymbol{v}_{r,ij}^{T} - \boldsymbol{p}_{r,ij}^{T} \right) (\boldsymbol{u}_{i} - \boldsymbol{u}_{ih,j}) + \kappa(h_{i}(\boldsymbol{p}_{i},\boldsymbol{v}_{i})) \right] \\
= \sup_{\boldsymbol{u}_{i},\boldsymbol{u}_{j}\in\mathbb{U}} \left[ -\frac{\|\boldsymbol{v}_{r,ij}\|\rho_{ij}\dot{\rho}_{ij}}{\sqrt{\|\boldsymbol{p}_{r,ij}\|^{2} - \rho_{ij}^{2}}} - \|\boldsymbol{p}_{r,ij}\|\|\boldsymbol{u}_{i}\|(\cos\phi_{r,ij}\cos<\boldsymbol{v}_{r,ij},\boldsymbol{u}_{i} > + \cos<\boldsymbol{p}_{r,ij},\boldsymbol{u}_{i} > \right) \\
+ \|\boldsymbol{p}_{r,ij}\|\|\boldsymbol{u}_{ih,j}\|(\cos\phi_{r,ij}\cos<\boldsymbol{v}_{r,ij},\boldsymbol{u}_{ih,j} > + \cos<\boldsymbol{p}_{r,ij},\boldsymbol{u}_{ih,j} > ) + \kappa(h_{i}(\boldsymbol{p}_{i},\boldsymbol{v}_{i})) \right] \\
= \sup_{\boldsymbol{u}_{i},\boldsymbol{u}_{j}\in\mathbb{U}} \left[ \frac{d\cos\phi_{r,ij}}{D_{s}^{d-1}} \frac{\|\boldsymbol{v}_{r,ij}\|^{2} \|\boldsymbol{p}_{r,ij}\|^{2(d-1)}}{\sqrt{D_{s}^{2(d-1)} - \|\boldsymbol{p}_{r,ij}\|^{2(d-1)}}} - \|\boldsymbol{p}_{r,ij}\|\|\boldsymbol{u}_{i}\|(\cos\phi_{r,ij}\cos<\boldsymbol{v}_{r,ij},\boldsymbol{u}_{i} > + \cos<\boldsymbol{p}_{r,ij},\boldsymbol{u}_{i} > + \cos<\boldsymbol{p}_{r,ij},\boldsymbol{u}_{i} > \right) \\
+ \|\boldsymbol{p}_{r,ij}\|\|\boldsymbol{u}_{th,j}\|(\cos\phi_{r,ij}\cos<\boldsymbol{v}_{r,ij},\boldsymbol{u}_{th,j} > + \cos<\boldsymbol{p}_{r,ij},\boldsymbol{u}_{th,j} > ) + \kappa(h_{i}(\boldsymbol{p}_{i},\boldsymbol{v}_{i})) \right]$$

It can be proved that  $u_i$  and  $u_{th,j}$  are on the plane spanned by  $p_{r,ij}$  and  $v_{r,ij}$  when (40) reaches the maximum according to the 3D geometry knowledge. In that way, here we select  $\langle v_{r,ij}, u_i \rangle = \pi - \phi_{r,ij} - \langle p_{r,ij}, u_i \rangle = \pi - \phi_{r,ij} - \langle p_{r,ij}, u_{th,j} \rangle = \pi - \phi_{r,ij} - \langle p_{r,ij}, u_{th,j} \rangle$ . And there is

$$\sup_{\boldsymbol{u}_{i},\boldsymbol{u}_{j}\in\mathbb{U}}\left[\dot{h}_{i}(\boldsymbol{p}_{r,ij},\boldsymbol{v}_{r,ij})+\kappa(h_{i}(\boldsymbol{p}_{r,ij},\boldsymbol{v}_{r,ij}))\right] \\
= \sup_{\boldsymbol{u}_{i},\boldsymbol{u}_{j}\in\mathbb{U}}\left[\frac{d\cos\phi_{r,ij}}{D_{s}^{d-1}}\frac{\left\|\boldsymbol{v}_{r,ij}\right\|^{2}\left\|\boldsymbol{p}_{r,ij}\right\|^{2(d-1)}}{\sqrt{D_{s}^{2(d-1)}-\left\|\boldsymbol{p}_{r,ij}\right\|^{2(d-1)}}}-\left\|\boldsymbol{u}_{i}\right\|(\left\|\boldsymbol{p}_{r,ij}\right\|\sin\phi_{r,ij})\sin(\phi_{r,ij}+\langle\boldsymbol{p}_{r,ij},\boldsymbol{u}_{i}\rangle) \\
+\left\|\boldsymbol{u}_{th,j}\right\|(\left\|\boldsymbol{p}_{r,ij}\right\|\sin\phi_{r,ij})\sin(\phi_{r,ij}+\langle\boldsymbol{p}_{r,ij},\boldsymbol{u}_{th,j}\rangle)+\kappa(h_{i}(\boldsymbol{p}_{i},\boldsymbol{v}_{i}))\right] \\
= \sup_{\boldsymbol{u}_{i},\boldsymbol{u}_{j}\in\mathbb{U}}\left[\frac{d\cos\phi_{r,ij}}{D_{s}^{d-1}}\frac{\left\|\boldsymbol{v}_{r,ij}\right\|^{2}\left\|\boldsymbol{p}_{r,ij}\right\|^{2(d-1)}}{\sqrt{D_{s}^{2(d-1)}-\left\|\boldsymbol{p}_{r,ij}\right\|^{2(d-1)}}}-\frac{\left\|\boldsymbol{p}_{r,ij}\right\|^{d}}{D_{s}^{d-1}}\left\|\boldsymbol{u}_{i}\right\|\sin(\phi_{r,ij}+\langle\boldsymbol{p}_{r,ij},\boldsymbol{u}_{i}\rangle) \\
-\frac{\left\|\boldsymbol{p}_{r,ij}\right\|^{d}}{D_{s}^{d-1}}\left\|\boldsymbol{u}_{th,j}\right\|\sin(\phi_{r,ij}+\langle\boldsymbol{p}_{r,ij},\boldsymbol{u}_{th,j}\rangle)+\kappa(h_{i}(\boldsymbol{p}_{i},\boldsymbol{v}_{i}))\right]$$

The threat tends to make the value of the above equation below to 0 to destroy the safety of UAV, while the UAV tries to make the value a positive one as larger as possible. Thus, it needs to analyze the safety situation when adopting the Min-Max strategy.

$$\sup_{\boldsymbol{u}_{i},\boldsymbol{u}_{j}\in\mathbb{U}}\left[\dot{h}_{i}(\boldsymbol{p}_{r,ij},\boldsymbol{v}_{r,ij}) + \kappa(h_{i}(\boldsymbol{p}_{r,ij},\boldsymbol{v}_{r,ij}))\right] \\
= \frac{\|\boldsymbol{p}_{r,ij}\|^{d}}{D_{s}^{d-1}}\left[\frac{d\cos\phi_{r,ij}\|\boldsymbol{v}_{r,ij}\|^{2}\|\boldsymbol{p}_{r,ij}\|^{d-2}}{\sqrt{D_{s}^{2(d-1)} - \|\boldsymbol{p}_{r,ij}\|^{2(d-1)}}} + \max(\|\boldsymbol{u}_{i}\|) - \max(\|\boldsymbol{u}_{th,j}\|)\right] + \kappa(h_{i}(\boldsymbol{p}_{i},\boldsymbol{v}_{i}))$$
(54)

Since the acceleration of UAV and the threat satisfies  $\max(||u_i||) > \max(||u_{th,j}||)$ , one can render that

$$\sup_{u_{i},u_{i}\in\mathbb{U}} [\dot{h}_{i}(p_{r,ij},v_{r,ij}) + \kappa(h_{i}(p_{r,ij},v_{r,ij}))] > 0$$
(55)

Thus, the proposed  $h_i(p_i, v_i)$  confirms to the definition and is a valid CBF. The proof completes here.

In the application, each UAV may encounter more than one threat during the flight, indicating that multiple constraints are introduced and the feasible region of the safety optimization problem may be a small and even empty one. Meanwhile, the conclusion of VO is yielded based on a linear motion with a constant velocity in a short time. That means the flight conflict prediction may be inconsistent with the realty and have a large error. Thus, the most imminent, to be precise the nearest threat with its corresponding safety constraint is taken into account for the penetration.

$$\begin{cases}
h_i(\boldsymbol{p}_{r,im}, \boldsymbol{v}_{r,im}) = \|\boldsymbol{p}_{r,im}\| \|\boldsymbol{v}_{r,im}\| \cos \phi_{r,im} + \boldsymbol{p}_{r,im}^T \boldsymbol{v}_{r,im} \\
m = \underset{j}{\operatorname{arg min}} (\|\boldsymbol{p}_{r,ij}\|)
\end{cases}$$
(56)

Next, the safety optimization problem can be solved. Select  $\kappa(h_i(\boldsymbol{p}_{r,im},\boldsymbol{v}_{r,im}))$  as  $\kappa h_i(\boldsymbol{p}_{r,im},\boldsymbol{v}_{r,im})$  with  $\kappa$  as a positive constant. Thus, the safety command of UAV i can be calculated by

$$\begin{cases}
\boldsymbol{u}_{i,safe} = -\frac{L_g h_i^T}{L_g h_i \cdot L_g h_i^T} \min(0, \ \psi_i(\boldsymbol{p}_{r,im}, \boldsymbol{v}_{r,im})) \\
\psi_i(\boldsymbol{p}_{r,im}, \boldsymbol{v}_{r,im}) = \dot{h}_i(\boldsymbol{p}_{r,im}, \boldsymbol{v}_{r,im}) + \kappa h_i(\boldsymbol{p}_{r,im}, \boldsymbol{v}_{r,im})
\end{cases}$$
(57)

And the total maneuver control input of UAV i is shown as follows

$$\boldsymbol{u}_{i} = \boldsymbol{u}_{i,safe} + \boldsymbol{u}_{i,nom} \tag{58}$$

#### 4. Simulation Analysis

To validate the effectiveness and superiority of the proposed approach, comparative simulations are carried out in this section. A UAV swarm encirclement scenario in the unbounded space is set with a group of noncooperative threats and a group of dynamic targets. In the scenario, due to the weak maneuver capability, the targets have no ability to perform some intense movements to escape the encirclement, and rely on the threats, which is in the friendly side for targets, to intercept the incoming UAVs. Here we consider the performance of the UAV and threats are not equal. Threats

have further detection range than UAV and will intercept once finding the UAV, whilst UAV has larger maximum acceleration to avoid the interception and achieve the penetration. Table 1 shows the parameters of the UAV, threats and targets.

Table 1 – Simulation Parameters

Parameters	Description	Value
$V_{uav,  { m max}}$	Maximum Speed of UAV	400 m/s
$a_{uav, \text{ max}}$	Maximum Acceleration of UAV	$30 \text{ m/s}^2$
$D_{com,uav}$	Communication Range of UAV	10000 m
$D_{det,uav}$	Detection Range of UAV	4000 m
$D_{safe,uav}$	Safety Range of UAV	40 m
$D_{bound}$	Thickness of Boundary Layer of Blockade Sphere	500 m
		1600 m
$K_{Bid}$	Positive Constant of Score Function	1
$k_{pn},k_{pp}$	Constants of Hawk-inspired Guidance	5, 5
$\kappa$ , $d$	Constants of Control Barrier Function	0.25, 0.5
au	Filter Time Constant of Time Coordination	0.5
$V_{thr,  \text{max}}$	Maximum Speed of Threat	350 m/s
$a_{thr, \max}$	Maximum Acceleration of Threat	$20 \text{ m/s}^2$
$D_{det, \; thr}$	Detection Range of Threat	6000 m
$D_{avoid, thr}$	Avoidance Range of Threat	1000 m
$K_{ap, thr}$	Constants of Attack Guidance	10
$K_{av, thr}$	Constants of Attack Guidance	8
$K_{sp, thr}$	Constants of Collision Avoidance Guidance	5
$V_{tg}$	Speed of Targets	10 m/s
_	Path Angle of Targets	0
χtg	Heading Angle of Targets	-45°
	$V_{uav, max}$ $a_{uav, max}$ $a_{uav, max}$ $D_{com, uav}$ $D_{det, uav}$ $D_{safe, uav}$ $D_{bound}$ $D_{nei}$ $K_{Bid}$ $k_{pn}, k_{pp}$ $\kappa, d$ $\tau$ $V_{thr, max}$ $a_{thr, max}$ $D_{det, thr}$ $D_{avoid, thr}$ $K_{ap, thr}$ $K_{av, thr}$ $K_{sp, thr}$ $V_{tg}$ $\gamma_{tg}$	$\begin{array}{cccccccccccccccccccccccccccccccccccc$

## 4.1 Fundamental Validation of Effectiveness

This part is a fundamental simulation to verify the effectiveness of the approach. Here 6 UAVs executes the cooperative encirclement of 16 targets, and 6 threats prevent the UAVs. The initial states of UAVs, threats and targets are randomly generated. Table 2 gives the allocation scheme of each UAV during the cooperative encirclement.

Table 2 – Encirclement allocation of the UAV swarm

ID	Anchor Point Allocation	Target Selection
UAV 1	4	8
UAV 2	5	1
UAV 3	6	3
UAV 4	2	12
UAV 5	1	11
UAV 6	3	7

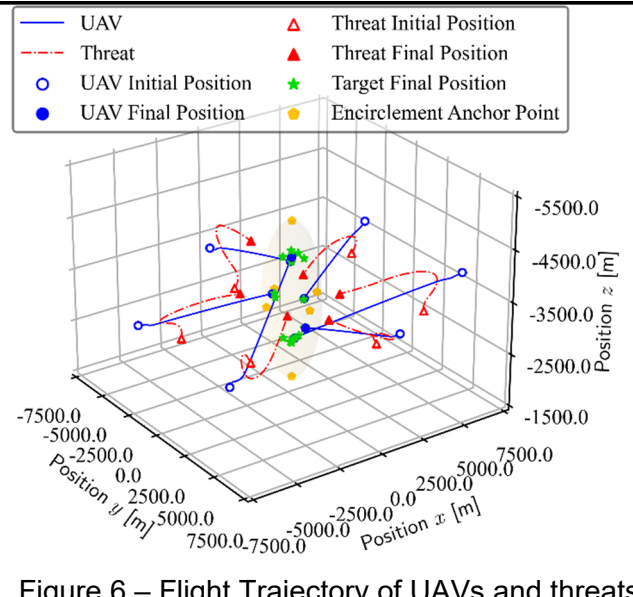


Figure 6 – Flight Trajectory of UAVs and threats

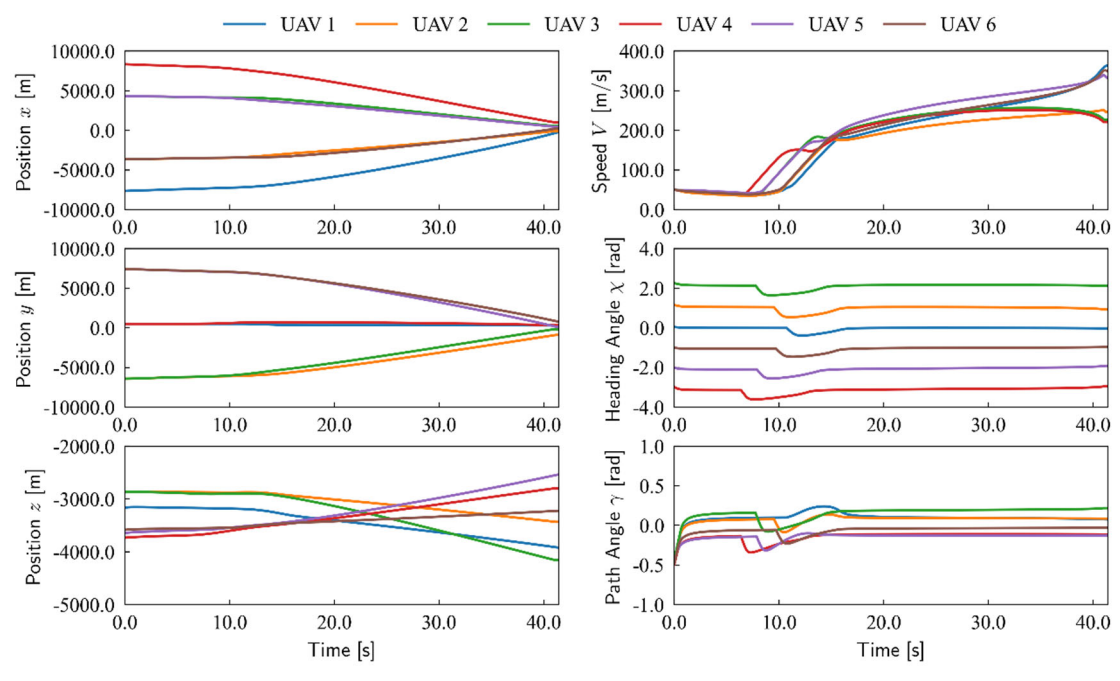


Figure 7 – UAV dynamics states variation with respect to time

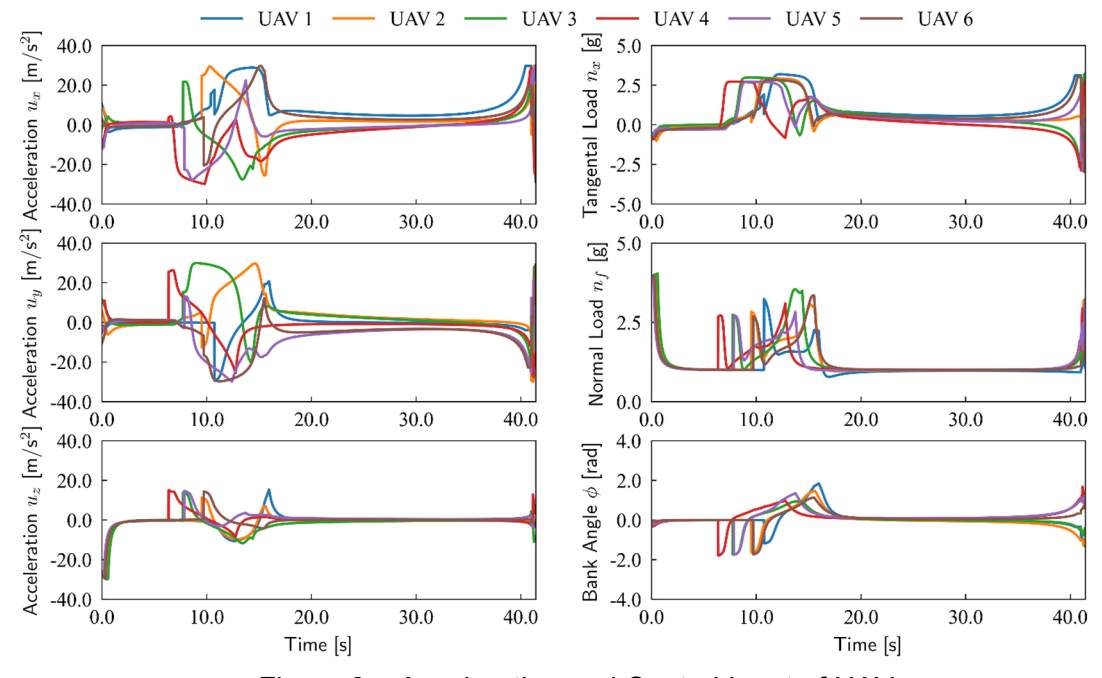


Figure 8 – Acceleration and Control Input of UAV

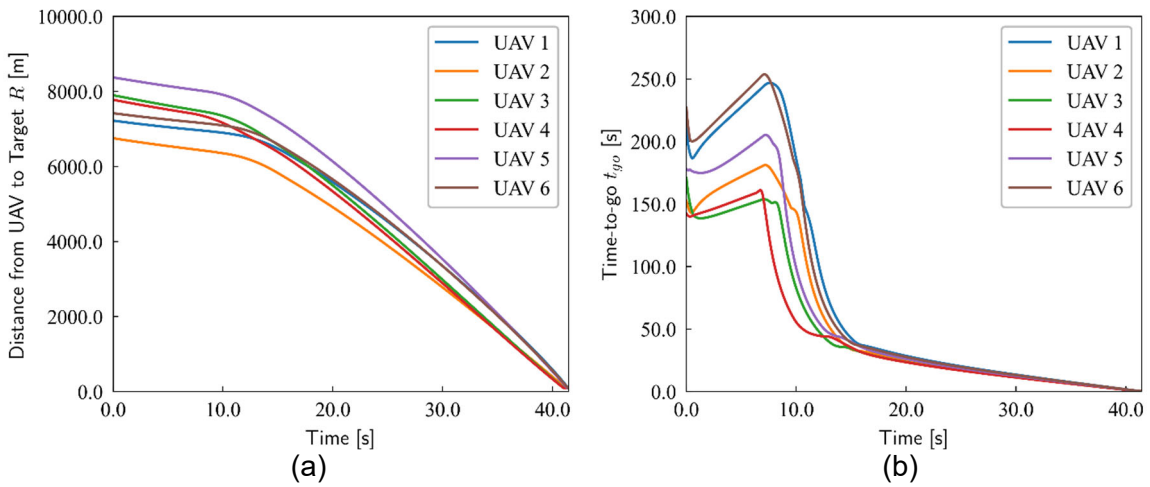


Figure 9 – Effectiveness of spatiotemporal synchronization of UAV swarm: (a) Distance from UAV to its target; (b) Time-to-go of each UAV

14

Figure 6 demonstrates the flight trajectory of each UAV and threat when the number of threats is equal to that of UAVs. And the states and control input are displayed in Figure 7. and 8, respectively.

Meanwhile, as Figure 9 shows, despite the different location, the UAV swarm succeeds in omnidirectional encirclement, attack the targets and achieve the spatial-temporal synchronization.

Moreover, when the UAV swarm tries to encircle the target groups, the avoidance maneuver occurs between UAVs and threats. It indicates that the UAV swarm drops into a noncooperative game with threats. Though the attack guidance of the threat, the UAVs break away from the interception and finally realize the penetration.

## 4.2 Comparison Simulation

This section mainly further proves the effectiveness from two aspects. First, the validity of the proposed approach is verified under the circumstance that the number of the threats is fewer than that of UAVs. Second, the approach superiority is illustrated by comparing with the existing methods.

Figure 5 (a) indicates the success of the swarm encirclement with 12 threats to intercept 6 UAVs. Though the number of threats is twice as much as that of UAVs and the cooperation among the threats is more significant, UAVs still realize the active avoidance and break through the multi-threat cooperative interception. The result indicates the adaptability and scalability of the scheme under different scales of threats.

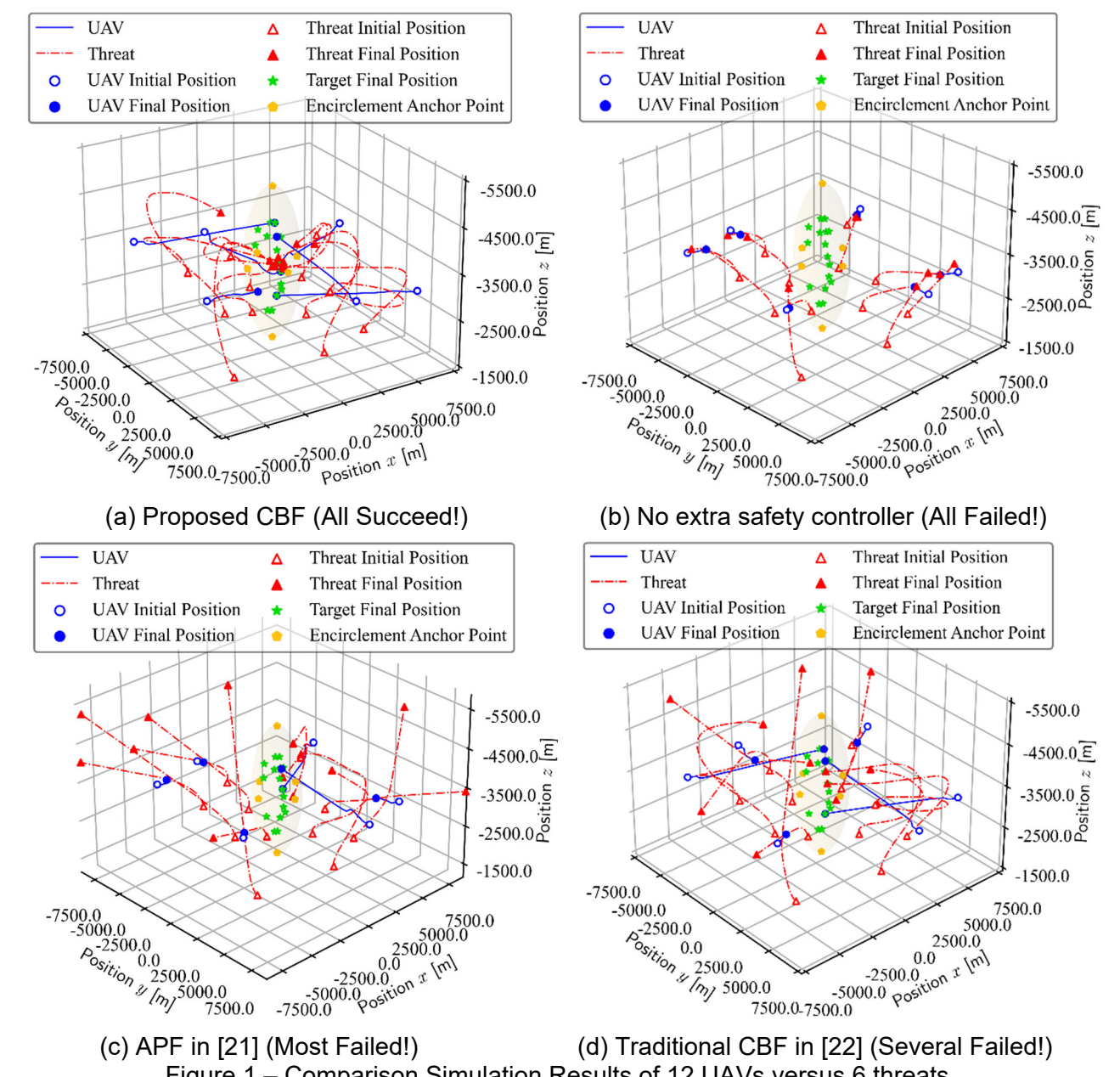


Figure 1 – Comparison Simulation Results of 12 UAVs versus 6 threats

Furthermore, the effectiveness of the safety strategy is more apparent by comparison with the

results under no extra safety steps, the APF-based strategy and traditional CBF-based strategy without threat behavior taken into account. In contrast to the failures of the above benchmarks shown

in Figure 5 (b), (c) and (d), all the UAVs complete its task by the proposed method. Thus, the approach is superior to the existing work when it comes to safety-critical penetration.

#### 5. Conclusion

In this paper, a hawk-inspired multi-layer framework is proposed in this work to guide the UAV swarm to encircle the target safely. It is the first attempt to study the safety-critical bionic cooperative guidance framework for the fixed-wing UAV swarm encirclement under constrained communication. Hawk-inspired tactics and pursuit law can achieve spatial-temporal synchronization. A novel kind of CBF is proposed and proved theoretically to guarantee flight safety and realize penetration. Numerical simulations indicate the proposed control scheme's feasibility and the UAV swarm can effectively break through the multi-threat interception and succeed in the cooperative encirclement. In the future, further research will focus on the safety-critical cooperative encirclement under the uncertain environment with incomplete awareness and limited information.

#### 6. Contact Author Email Address

mailto: byqin@mail.nwpu.edu.cn

## 7. Copyright Statement

The authors confirm that they, and/or their company or organization, hold copyright on all of the original material included in this paper. The authors also confirm that they have obtained permission, from the copyright holder of any third party material included in this paper, to publish it as part of their paper. The authors confirm that they give permission, or have obtained permission from the copyright holder of this paper, for the publication and distribution of this paper as part of the ICAS proceedings or as individual off-prints from the proceedings.

#### References

- [1] Yang XU, Yuanfang QU, Delin LUO and et.al. Distributed Fixed-time Time-varying Formation-containment Control for Networked Underactuated Quadrotor UAVs with Unknown Disturbances. *Aerospace Science and Technology*, Vol. 130, No. 107909, 2022.
- [2] Boyu QIN, Dong ZHANG, Shuo TANG and Mengyang WANG. Distributed Grouping Cooperative Dynamic Task Assignment Method of UAV Swarm. *Applied Sciences-Basel*, Vol. 12, No. 2865, 2022.
- [3] Boyu QIN, Dong ZHANG, Shuo TANG and Yang XU. Two-Layer Formation-Containment Fault-Tolerant Control of Fixed-Wing UAV Swarm for Dynamic Target Tracking. *Journal of Systems Engineering and Electronics*, Vol. 34, No. 6, pp 1375-1396, 2023.
- [4] F. Mehdifar, C. P. Bechlioulis, J. M. Hendrickx, and D. V. Dimarogonas. 2-D Directed Formation Control Based on Bipolar Coordinates. *IEEE Transactions on Automatic Control*, Vol. 68, No. 7, pp 4175–4190, 2023.
- [5] Jiangbo JIA, Xin CHEN, Weizhen WANG, and Min ZHANG. Distributed Control of Target Cooperative Encirclement and Tracking Using Range-Based Measurements. *Asian Journal of Control*, Vol. 25, No. 6, pp 4595-4608, 2023.
- [6] Jianglong YU, Xiwang DONG, Qingdong LI, and Zhang REN. Distributed Cooperative Encirclement Hunting Guidance for Multiple Flight Vehicles System. *Aerospace Science and Technology*, Vol. 95, No. 105475, 2020.
- [7] Aiwu YANG, Xiaolong LIANG, Yueqi HOU, and Maolong LV. An Autonomous Cooperative Interception Method with Angle Constraints Using a Swarm of UAVs. *IEEE Transactions on Vehicular Technology*, Vol. 72, No. 12, pp 15436-15449, 2023.
- [8] Garcia, E; Bopardikar, S.D. Cooperative Containment of a High-speed Evader. 2021 American Control Conference (ACC). pp 4698-4703, 2021.
- [9] Mengda JI, Genjiu XU, Zekun DUAN, et al. Cooperative Pursuit with Multiple Pursuers Based on Deep Minimax Q-learning. *Aerospace Science and Technology*, Vol. 146, No. 108919, 2024.
- [10]C. H. Brighton, A. L. R. Thomas, and G. K. Taylor. Terminal Attack Trajectories of Peregrine Falcons Are Described by the Proportional Navigation Guidance Law of Missiles. *Proceedings of the National Academy of Sciences.*, Vol. 114, No. 51, pp. 13495–13500, 2017.
- [11]Zhu WANG, Li LIU, Teng LONG. Minimum-Time Trajectory Planning for Multi-Unmanned-Aerial-Vehicle Cooperation Using Sequential Convex Programming. *Journal of Guidance, Control, and Dynamics*, vol. 40, No.11, pp 2976-2982, 2017.
- [12]Xiangru XU., Tabuada, P., Grizzle, J. W, et al. Robustness of Control Barrier Functions for Safety-critical Control. *IFAC-PapersOnLine*, Vol. 48, No. 27, pp 54-61, 2015.
- [13]Singletary A, Kolathaya S, Ames A D. Safety-critical Kinematic Control of Robotic Systems. IEEE Control

- Systems Letters, Vol. 6, pp 139-144, 2021.
- [14]Xiaowei FU, Jing PAN, Haixiang WANG, et al. A Formation Maintenance and Reconstruction Method of UAV swarm Based on Distributed Control. *Aerospace Science and Technology*, Vol. 104, No. 105981, 2020.
- [15]Demšar J, Hemelrijk C K, Hildenbrandt H, et al. Simulating Predator Attacks on Schools: Evolving Composite Tactics. *Ecological Modelling*, Vol. 304, pp. 22–33, 2015.
- [16]Wanying RUAN, Yongbin SUN, Yimin DENG, and Haibin DUAN. Hawk-Pigeon Game Tactics for Unmanned Aerial Vehicle Swarm Target Defense. *IEEE Transactions on Industrial Informatics*, Vol. 19, No. 12, pp 11619-11629, 2023.
- [17]Brighton C H, and Taylor G K. Hawks Steer Attacks Using A Guidance System Tuned for Close Pursuit of Erratically Manoeuvring Targets. *Nature Communications*, Vol 10, No. 2462, 2019.
- [18]Zhuozhu JIAN, Zihong YAN, Xuanang LEI, et al. Dynamic Control Barrier Function-based Model Predictive Control to Safety-Critical Obstacle-Avoidance of Mobile Robot. 2023 IEEE International Conference on Robotics and Automation (ICRA), pp. 3679-3685, 2023.
- [19]J ZENG, B ZHANG, Sreenath K. Safety-Critical Model Predictive Control with Discrete-Time Control Barrier Function. 2021 American Control Conference (ACC). pp 3882-3889, 2021.
- [20]Squires E, Pierpaoli P, Konda R, et al. Composition of safety constraints for fixed-wing collision avoidance amidst limited communications[J]. *Journal of Guidance, Control, and Dynamics*, Vol. 45, No. 4, pp 714-725, 2022.
- [21] Yang XU, Delin LUO, Dongyu LI, et al. Target-Enclosing Affine Formation Control of Two-Layer Networked Spacecraft with Collision Avoidance. *Chinese Journal of Aeronautics*, Vol. 32, No. 12, pp 2679-2693, 2019.
- [22]Thontepu P, Goswami B G, Tayal M, et al. Collision Cone Control Barrier Functions for Kinematic Obstacle Avoidance in UGVs. 2023 Ninth Indian Control Conference (ICC), pp 293-298, 2023.